

# Type Ia supernovae from non-accreting progenitors

J. Antoniadis<sup>1,2</sup>, S. Chanlaridis<sup>2</sup>, G. Gräfener<sup>2</sup>, and N. Langer<sup>2,1</sup>

<sup>1</sup> Max Planck Institut für Radioastronomie Auf dem Hügel 69, 53121, Bonn, Germany

<sup>2</sup> Argelander Institut für Astronomie, Auf dem Hügel 71, 53121, Bonn, Germany  
e-mail: jantoniadis@mpi-fr-bonn.mpg.de

January 22, 2020

## ABSTRACT

Type Ia supernovae (SNe Ia) are manifestations of stars deficient of hydrogen and helium disrupting in a thermonuclear runaway. While explosions of carbon-oxygen white dwarfs are thought to account for the majority of events, part of the observed diversity may be due to varied progenitor channels. We demonstrate that helium stars with masses between  $\sim 1.8$  and  $2.5 M_{\odot}$  may evolve into highly degenerate, near-Chandrasekhar mass cores with helium-free envelopes that subsequently ignite carbon and oxygen explosively at densities  $\sim (1.8 - 5.9) \times 10^9 \text{ g cm}^{-3}$ . This happens either due to core growth from shell burning (when the core has a hybrid CO/NeO composition), or following ignition of residual carbon triggered by exothermic electron captures on  $^{24}\text{Mg}$  (for a NeOMg-dominated composition). We argue that the resulting thermonuclear runaways is likely to prevent core collapse, leading to the complete disruption of the star. The available nuclear energy at the onset of explosive oxygen burning suffices to create ejecta with a kinetic energy of  $\sim 10^{51}$  erg, as in typical SNe Ia. Conversely, if these runaways result in partial disruptions, the corresponding transients would resemble SN Iax events similar to SN 2002cx. If helium stars in this mass range indeed explode as SNe Ia, then the frequency of events would be comparable to the observed SN Ib/c rates, thereby sufficing to account for the majority of SNe Ia in star-forming galaxies.

**Key words.** binaries: general - stars: evolution - supernovae: general

## 1. Introduction

Despite their central role in Astrophysics and Cosmology, the origin and physics of Type Ia supernovae (SNe Ia) remain uncertain (Maoz et al. 2014). Typical SNe Ia luminosities ( $\sim 10^{43} \text{ erg s}^{-1}$ ) and ejecta velocities ( $\sim 10^4 \text{ km s}^{-1}$ ), require  $^{56}\text{Ni}$  masses and kinetic energies of order  $\sim 0.6 M_{\odot}$  and  $\sim 10^{51}$  erg respectively. These properties suggest that SNe Ia are most likely stars that disrupt in thermonuclear explosions, rather than core-collapse events. Carbon/oxygen white dwarfs (CO WDs) approaching the Chandrasekhar-mass limit ( $M_{\text{Ch}}$ ) are the most promising progenitor systems, as they can produce explosions broadly consistent with observations (Nomoto 1982; Wang & Han 2012; Churazov et al. 2014).

Conventional stellar evolution channels, produce stable CO WDs with masses below  $\sim 1.1 M_{\odot}$ . Consequently, matter accretion onto the WD is required to trigger an explosion, either via stable transfer from a donor star (single-degenerate channels; SD), or in a merger event (double-degenerate and core-degenerate channels; DD and CD). Thus far, all of the binary models encounter substantial difficulties in providing a self-consistent model for SNe Ia (Livio & Mazzali 2018; Soker 2019). For instance, SD channels require considerable fine-tuning of the mass accretion rate for the WD to grow in mass. In addition, the interaction between the SN blast and the donor star or the circumbinary material, is expected to produce signatures which are rarely or never seen, e.g. some contribution to the SN luminosity at early times (Kasen 2010), radio synchrotron emission (Harris et al. 2016), and  $H\alpha$  emission due to unburned hydrogen. DD mergers on the other hand may produce a variety of outcomes, ranging from prompt explosions to long-lived remnants, or the delayed formation of a neutron star (Livio & Mazzali 2018). In addition, their overall contribution to the

observed SNe Ia rate may be too low (van Kerkwijk et al. 2010; Claeys et al. 2014a; Sato et al. 2015).

Over the past 50 years, systematic studies of SNe Ia explosions have revealed a large diversity in their properties (Taubenberger 2017). Notable outliers include luminous (e.g. SN 1991T; Filippenko et al. 1992) and ultra-luminous (e.g. SNLS-03D3bb; Howell et al. 2006) SNe; SN 1991bg-like transients which are faint and fast evolving (Ruiz-Lapuente et al. 1993); peculiar SN 2002cx-like SNe, also known as SNe Iax, that may be pure thermonuclear deflagrations of helium-deficient compact objects (e.g. Li et al. 2003; Branch et al. 2004; Magee et al. 2016; Jha 2017; Magee et al. 2019) and SN 2012ca-like events, dubbed SNe Ia-CSM, for which there is evidence for interaction with a dense circum-stellar medium (Bochenek et al. 2018). Even among “normal” SNe Ia there is appreciable scatter in rise times, maximum luminosities, ejecta velocities and spectral evolution (Livio & Mazzali 2018). Finally, there seems to be a correlation with environment, as star-forming galaxies typically host more, and brighter SNe Ia (Maoz et al. 2014).

While part of this diversity can be understood within the framework of SD and DD/CD families, there may exist additional evolutionary pathways leading to SNe Ia. It is known since long that intermediate-mass stars form degenerate cores after helium burning which may ignite carbon explosively if the core mass is allowed to grow due to shell burning (Rose 1969; Arnett 1969; Wheeler 1978). This scenario became unlikely when it was made clear that the loss of the hydrogen envelope during the AGB evolution ends the core growth rather early, which can only potentially be prevented in the most massive AGB stars (see Iben & Renzini 1983, and references therein). In this case, however, the emerging supernova would be a H- and He-rich “SNe 1.5”. Waldman & Barkat (2006) and Waldman et al. (2008)

have considered the possible connection between ONe cores and SNe Ia in more detail, demonstrating that some helium stars with (C)NeO cores can explode before any significant deleptonization due to electron captures on  $^{20}\text{Ne}$  occurs. Their models still retain a small He-rich envelope at the end and therefore, it is again unclear if such transients would appear as classical SNe Ia.

In spite of the aforementioned works, ONe cores are generally thought to produce massive WDs or core-collapse electron-capture supernovae (ECSNe; e.g., [Nomoto & Kondo 1991](#); [Gutierrez et al. 1996](#); [Takahashi et al. 2013](#)). However, recent three-dimensional hydrodynamical simulations of oxygen deflagrations in ONe cores at central densities  $\geq 10^{10} \text{ g cm}^{-3}$ , *viz.* after the onset of electron-captures on  $^{20}\text{Ne}$ , suggest that a large fraction of the star ( $\geq 1 M_{\odot}$ ) may be ejected in a so-called thermonuclear ECSN, leaving behind only a small bound remnant ([Jones et al. 2016, 2019](#)).

In light of these results, we revisit the work of [Waldman & Barkat \(2006\)](#) and [Waldman et al. \(2008\)](#) using modern tools and updated input physics. We demonstrate that a thermonuclear runaway leading to a SN Ia can indeed be initiated during the late evolution of a degenerate core of neon-oxygen (NeO) or carbon-neon-oxygen (CNeO) composition as it approaches  $M_{\text{Ch}}$ . We show that near- $M_{\text{Ch}}$  (C)NeO cores originating from intermediate mass helium stars ( $\sim 1.8 - 2.5 M_{\odot}$ ) — a common product of binary interactions — can ignite their residual carbon and oxygen explosively at densities  $\lesssim 6 \times 10^9 \text{ g cm}^{-3}$ , before the onset of  $^{20}\text{Ne}(e^{-}, \nu_e)^{20}\text{F}$  electron-capture reactions at  $\sim 10^{10} \text{ g cm}^{-3}$  (Section 2). In addition, during the final evolutionary stages, the envelope inflates significantly and is lost promptly via winds or due to binary interaction. Consequently, the star is helium free when brought to thermonuclear explosion. The available nuclear energy at the time of central oxygen ignition suffices to unbind the star and to yield ejecta with kinetic energies comparable to what is expected for classical SNe Ia (Section 2.5). This mechanism does not require accretion from the binary companion and therefore may contribute significantly to the SN Ia rate in young stellar populations (Section 3).

## 2. (C)NeO cores: formation and evolution

### 2.1. Overview

Degenerate stellar cores of NeO composition form inside stars with ZAMS masses between  $\sim 7$  and  $11 M_{\odot}$  (e.g. [Poelarends 2007](#); [Poelarends et al. 2008](#); [Farmer et al. 2015](#)). After core helium burning, such stars enter a super-asymptotic giant branch (SAGB) phase, characterized by a dense CO core and an extended hydrogen envelope. As the core becomes increasingly more degenerate, it cools substantially due thermal neutrino emission. An important consequence is that the critical temperature for  $^{12}\text{C}$  ignition is first attained off-center, creating a turbulent flame that propagates inwards ([Siess 2006](#)).

Carbon burning in SAGB stars may be affected by complex mixing processes due to a combination of inverse composition gradients, overshooting, semi-convection and rotation. The penetration of Ne/O/Na/Mg ashes into unburned regions, may impact significantly the propagation of the burning front. Mixing generally reduces the rate of thermonuclear reactions, leaving behind substantial amounts of residual carbon. In extreme cases, the flame can be quenched completely, resulting in a hybrid structure, with a CO core, surrounded by a NeO mantle ([Denis-Senkov et al. 2013](#)).

The subsequent evolution and final fate of such stars depends critically on the competition between neutrino cooling due to

the presence of  $^{23}\text{Na}^{23}\text{Ne}$  and  $^{25}\text{Mg}^{25}\text{Na}$  Urca pairs, and compressional heating due to core growth from the helium burning shell ([Schwab et al. 2017](#)). SAGB stars are subject to significant dredge-up and thermally unstable shell burning. These effects may impact substantially the ability of the core to grow in mass fast enough.

However, thermal pulses and dredge-up episodes do not occur when the hydrogen envelope is lost, e.g. due to strong winds, or via interactions in a multiple system ([Poelarends 2007](#); [Poelarends et al. 2008](#); [Woosley 2019](#)). In such a case, helium shell burning is stable, allowing the core to approach the Chandrasekhar mass limit. In what follows, we build detailed numerical models to investigate the combined effects of residual unburned  $^{12}\text{C}$ , Urca cooling and constant mass growth from shell burning, in the late evolution of (C)NeO cores that originate from helium stars.

### 2.2. Numerical Calculations: Input Physics

We use MESA (version 10386) to follow the evolution of two helium-star models, m1 and m2, with masses of  $2.5$  and  $1.8 M_{\odot}$  respectively. The initial models have uniform compositions with  $Y = 0.98$  and  $Z = 0.02$  (solar abundances are taken from [Grevesse & Sauval 1998](#)). We employ a nuclear network that considers 43 isotopes, from  $^1\text{H}$  to  $^{58}\text{Ni}$ . Reaction rates are based on the JINA reacLib v2.0 compilation ([Cyburt et al. 2010](#)). Electron screening factors and cooling rates from thermal neutrinos are evaluated as in [Farmer et al. \(2015\)](#), and references therein. Weak interaction rates are taken from [Suzuki et al. \(2016\)](#). Wind mass-loss rates are calculated using MESA’s Dutch compilation of recipes ([Paxton et al. 2013](#)), which is composition-independent. We use “Type 2” opacities during and after core helium burning.

Our baseline model considers convection, thermohaline and semi-convective mixing. Convective stability is evaluated using the Ledoux criterion. By default, MESA uses standard mixing-length theory (MTL; [Cox & Giuli 1968](#)) for convective mixing and energy transport. However, following carbon burning, both our models develop dynamically-unstable super-Eddington envelopes, causing numerical difficulties. For this reason, we decided to employ the “enhanced” MLT option available in MESA ([Paxton et al. 2013](#)), which artificially reduces the super-adiabatic gradient leading to an enhanced convective energy transport efficiency. This allows us to follow the evolution of the core after carbon burning without interruptions. We further discuss this choice and its impact on the envelope evolution and the final mass in Section 4. The MLT mixing length parameter is set to  $a_{\text{MLT}} = 2.0$  for both models. For thermohaline mixing we employ the [Kippenhahn et al. \(1980\)](#) treatment, setting  $D_{\text{TH}} = 1.0$  for the diffusion coefficient. Semi-convection is evaluated following [Langer et al. \(1983\)](#), adopting an efficiency parameter of  $\alpha_{\text{SEM}} = 1.0$ . Our models do not employ the predictive convective boundary mixing approach described in [Paxton et al. \(2018\)](#).

While m1 does not consider the effects of convective overshoot ( $f_{\text{ov}} = 0.0$ ), in m2, we set  $f_{\text{ov}} = 0.014$  across all convective boundaries, including the base of the carbon-burning flame. While mixing at this interface is unlikely ([Lecoanet et al. 2016](#)), we use this as a means to quench the flame before it reaches the center. Other processes such as rotation and thermohaline mixing can lead to the same outcome for similar initial helium core masses ([Farmer et al. 2015](#)). The MESA inlists are publicly available<sup>1</sup>. An extended grid exploring a broad range of initial

<sup>1</sup> <https://zenodo.org/record/3580243#.XfjNjpnKJUI>

masses, metallicities, overshooting and wind parameters will be presented in an accompanying paper (Chanlaridis et al. 2019).

### 2.3. Simulation results

Figure 1 shows Kippenhahn diagrams for m1 and m2, focusing on the evolution after central helium depletion. m1 first ignites carbon at mass coordinate  $\sim 0.3 M_{\odot}$ , when the total mass is  $2.25 M_{\odot}$ , and the CO core has a mass of  $\sim 1.15 M_{\odot}$ . The initial flame is followed by secondary flashes propagating in both directions. Some of these episodes seem to occur only after a small critical mass of carbon has been accumulated below the burning shell. The entire carbon-burning phase lasts for about 40,000 yr. During most of this time, the star is a red giant with a low-density convective envelope ( $R \simeq 125 R_{\odot}$ ,  $\log_{10}(T_{\text{eff}}/\text{K}) \simeq 3.75$ ,  $\log_{10}(L/L_{\odot}) \simeq 4.3$ ), and loses mass at a rate of  $\dot{M} \simeq 10^{-6} M_{\odot} \text{ yr}^{-1}$ , in good agreement with the recent KEPLER models (Woosley 2019), which employ the mass-loss scheme of Yoon (2017), more specifically targeted to helium stars. While the mass-loss strength is highly uncertain, it has recently been suggested that the winds during the helium and carbon burning phases in low-mass helium stars may be less powerful than the Dutch schemes predict, given that Wolf-Rayet stars are not seen in this mass range (Gräfener et al. 2017; Vink 2017). In such a case, the cores in our models could grow faster.

As the core contracts and its surface gravity increases, the surrounding burning shells become progressively thinner. The envelope responds by expanding and the stellar structure resembles closely that of an SAGB core. Interestingly, Woosley (2019) finds that only helium stars with masses between  $\sim 1.6$  and  $3.2 M_{\odot}$ , develop sufficiently thin helium-burning shells to cause envelope inflation. Hence, higher-mass stars would likely retain a significant fraction of outer layer until the end, leading to Type Ib SN explosions.

The last  $\sim 5,000$  yr of the evolution are characterized by vigorous burning in two neighbouring shells which eventually merge, resulting in violent burning, at  $t \simeq 2.41$  Myr (Figure 1). In this phase, the star reaches extremely high luminosities up to  $\log L/L_{\odot} = 6.25$ , generating a strong stellar wind that lasts for  $\sim 3000$  yr and eventually removes the remaining He-rich envelope. The evolution of the envelope during this stage depends critically on the energy transport mechanism above Eddington luminosities. With the enhanced MLT option employed in our calculations, m1 briefly becomes a yellow supergiant as the envelope expands to  $R \simeq 900 R_{\odot}$  while remaining dynamically stable. The resulting strong wind of  $\dot{M} \simeq 10^{-3.8} M_{\odot} \text{ yr}^{-1}$  is in the same range as theoretically expected maximum values for super-Eddington outflows (Owocki et al. 2004; Smith & Owocki 2006). Conversely, using standard MLT, the envelope becomes dynamically unstable and our calculations encounter numerical difficulties just as the star leaves its Hayashi track, when the core has a mass of  $1.32 M_{\odot}$ . By extrapolating the core-growth rate, the core of the star would likely still reach  $M_{\text{Ch}}$ . As our helium star may be the product of close binary evolution, at this stage further interactions would easily remove the envelope, as its binding energy corresponds to only a minuscule fraction of the orbital energy reservoir.

Either way, the combination of enhanced mass loss from both winds and binary interaction and vigorous burning, leads to the complete depletion of helium in the envelope. Following the neon flash, the small residual envelope contracts and the wind ceases completely for the last  $\sim 5,000$  yr (Figure 1). Our model stops when the star has a mass of  $1.39 M_{\odot}$  (see Sec. 2.4).

The evolution of the envelope in m2 is similar (Figure 1). Here, the star expands twice, first for  $\sim 5,000$  yr ( $t = 5.005$  Myr in Figure 1) and then again briefly for some  $\sim 500$  yr ( $t = 5.015$  Myr), reaching a maximum size of  $300 R_{\odot}$ . The mass-loss rate mostly remains below  $10^{-6} M_{\odot} \text{ yr}^{-1}$ . In m2, carbon ignites near mass coordinate  $1.1 M_{\odot}$ , just as the star begins to develop an SAGB structure. The flame is quenched after only  $0.1 M_{\odot}$  of material has been converted to NeO, leaving behind a hybrid CO/NeO structure. Without overshooting, the flame propagates all the way to the center, converting the entire core to ONe (see model m2b in Figure 1). The final mass of m2 (and m2b) is  $1.37 M_{\odot}$ .

To summarise, during the final evolutionary stages, both models are helium depleted and nearing  $M_{\text{Ch}}$ . The ability of the core to grow in mass depends somewhat on the uncertain mass-loss rate during the final burning phases. If the envelope is lost too early during the SAGB phase (which does not seem to be the case), then the two stars would leave behind white dwarfs with masses  $\leq 1.38 M_{\odot}$ , and ONe and CO/ONe composition respectively. Conversely, if the envelope is retained for long enough, as we find in our models, then the central density increases sufficiently to trigger either electron captures on  $^{24}\text{Mg}$  or central carbon ignition. In the following section we examine the evolution of the core during this phase.

### 2.4. Oxygen ignition and thermonuclear runaway

Figure 2 gives an overview of the central density and temperature evolution for models m1 and m2. Following the main carbon-burning episode, both stars continue to contract, while cooling due to neutrino emission. As shell burning intensifies, compressional heating eventually balances off neutrino losses, at  $\log_{10}(\rho_c/\text{g cm}^{-3}) \simeq 8.3$  and  $8.0$  for m1 and m2 respectively. The subsequent evolution depends on the composition.

For m1, the degenerate core is composed mostly of neon and oxygen. The most abundant isotopes have  $X(^{16}\text{O}) \simeq 0.43$ ;  $X(^{20}\text{Ne}) \simeq 0.42$ ;  $X(^{24}\text{Mg}) \simeq 0.1$ ;  $X(^{12}\text{C}) \simeq 0.011$ ;  $X(^{23}\text{Na}) \simeq 0.037$ ;  $X(^{25}\text{Mg}) \simeq 0.001$ . Between  $\log_{10}(\rho_c/\text{g cm}^{-3}) = 9.05$  and  $9.25$ , the temperature drops to  $\log_{10}(T_c/\text{K}) \simeq 8.2$  due to  $^{25}\text{Mg}^{25}\text{Na}$  and  $^{23}\text{Na}^{23}\text{Na}$  direct Urca reactions. At higher densities, neutrino cooling ceases completely, and the temperature rises again (Figure 2). When  $\log_{10}(\rho_c/\text{g cm}^{-3}) = 9.65$ , exothermic electron captures on  $^{24}\text{Mg}$  and  $^{24}\text{Na}$  start occurring at a substantial rate, raising the temperature adequately to ignite carbon. In turn, this triggers oxygen burning and a thermonuclear runaway at  $\log_{10}(\rho_c/\text{g cm}^{-3}) = 9.77$ . This ignition density is lower than the  $\log_{10}(\rho_c/\text{g cm}^{-3}) \geq 9.97$  typically expected for oxygen deflagrations in pure NeO cores (Jones et al. 2019). As a consequence, severe deleptonization due to  $^{20}\text{Ne}$  electron captures is likely avoided. To demonstrate the importance of residual carbon, we computed a variation of this model in which the energy contribution of all carbon-consuming reactions is artificially suppressed following the main carbon-burning phase (model m1b in Figure 2). In this case, oxygen ignites above  $\log_{10}(\rho_c/\text{g cm}^{-3}) \simeq 10$  and only after  $^{20}\text{Ne}$  electron captures have started to occur at a significant rate. Hence, in the absence of residual carbon, this star would produce a core-collapse or a thermonuclear ECSN (Jones et al. 2016).

m2 is composed mostly of carbon and oxygen, with  $X(^{12}\text{C}) = 0.38$  and  $X(^{16}\text{O}) = 0.60$  respectively. Here,  $^{23}\text{Na}$  is not abundant enough to cause substantial cooling. Consequently, carbon, which is significantly more abundant compared to m1, ignites at  $\log_{10}(\rho_c/\text{g cm}^{-3}) = 9.26$ .

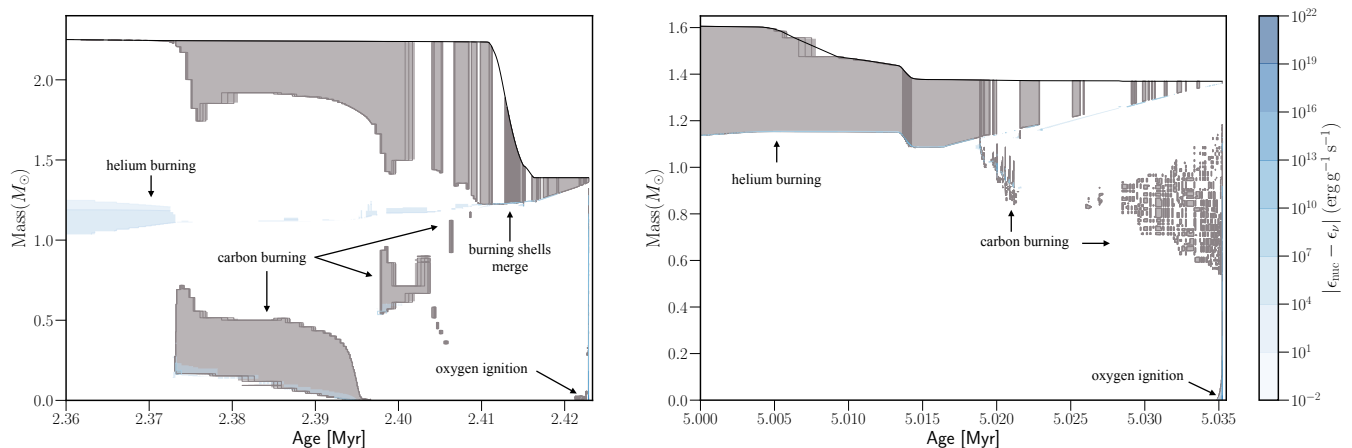


**Fig. 1.** Kippenhahn diagrams following the evolution of m1 (left) and m2 after core helium depletion. Blue-shaded areas indicate regions in which nuclear burning occurs, i.e. locations for which the nuclear energy  $\epsilon_{\text{nuc}}$  exceeds energy losses due to neutrino emission,  $\epsilon_{\nu}$ . Gray regions are subject to convective mixing.  $t = 0$  corresponds to the onset of core helium burning.

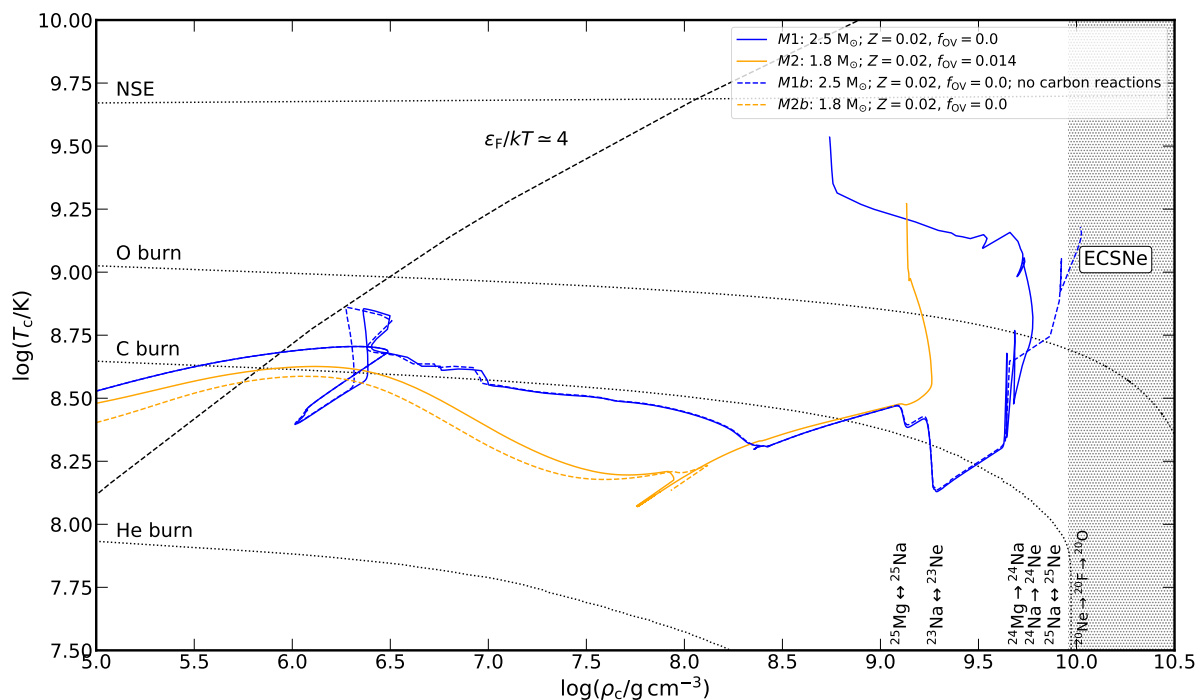


**Fig. 2.** Evolution of the core density and temperature for m1 and m2. The dashed line shows the approximate boundary for electron degeneracy. Burning thresholds for a 100% abundance of the corresponding species are indicated with dotted lines. The NSE threshold assumes an equilibrium timescale of 1 s. In model m1b, the energy contribution of carbon-consuming reactions is set to zero (see text). M2b shows the core evolution of a  $1.8 M_{\odot}$  without overshooting. While this model stopped at  $\log_{10}(\rho_c/g \text{ cm}^{-3}) \approx 8.2$  due to numerical convergence issues, the final core mass is similar to m2.

The evolution following central oxygen ignition is not adequately modeled in our 1D simulations. m2 will most likely disrupt in a SNIa, as the composition and ignition conditions resemble closely those found in standard CO WD SNIa progenitors (Nomoto 1982). While the fate of m1 is less certain, a thermonuclear explosion is also the most likely outcome: firstly,

the available nuclear energy is sufficient to unbind the star (see below). Secondly, the ignition density is only slightly higher than what is typically considered for CO WD SNIa progenitors. Hence, the deflagration ashes will likely be buoyant, leading to expansion, which will in turn limit the deleptonization rate. This hypothesis is strongly supported by 3D hydrodynamic simula-



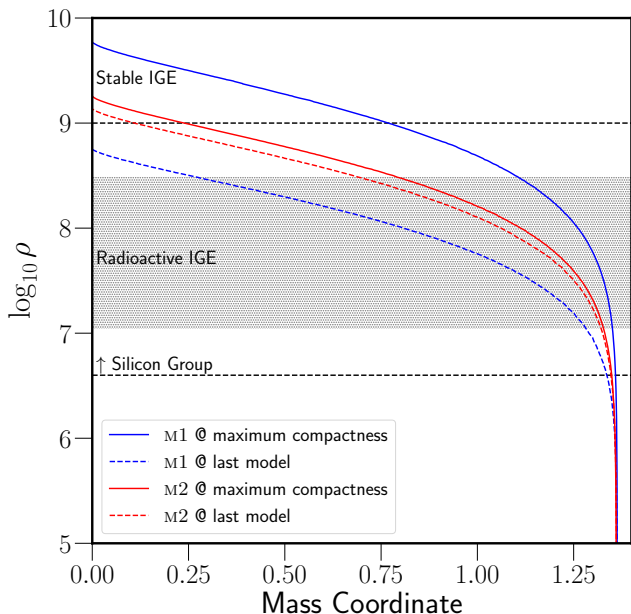


**Fig. 3.** Density profiles at maximum compactness (solid lines) and at the end of our MESA calculations (dashed lines). Regions indicating approximate burning regimes as in [Seitenzahl & Townsley \(2017\)](#).

tions of ECSN deflagrations by [Jones et al. \(2016, 2019\)](#): their least compact progenitor ignites at  $\log_{10}(\rho_c/\text{g cm}^{-3}) = 9.90$  but still manages to eject  $\sim 1 M_{\odot}$  of material. Similarly, [Marquardt et al. \(2015\)](#) simulate ONe WD detonations at lower densities and demonstrate that the explosion is practically identical to a typical SN Ia. Interestingly in our 1D simulations, both models experience significant expansion. This is most likely the result of (over-)efficient convection, which also homogenizes the inner  $\sim 1 M_{\odot}$  of the core.

### 2.5. Energetics and nucleosynthesis

Figure 3 shows the density profiles of m1 and m2 at maximum compactness ( $\log_{10}(\rho_c/\text{g cm}^{-3}) = 9.77$  and  $9.22$ , respectively), and at the end of our simulations. At the onset of oxygen ignition, m1 and m2 have binding energies of  $E_{\text{bind}} = -5.76 \times 10^{50}$  and  $-5.16 \times 10^{50}$  erg, and average electron fractions of  $Y_e = 0.496$  and  $0.499$ , respectively. If these progenitors were to produce an SN Ia of typical composition, with  $\sim 0.7 M_{\odot}$  of nickel and iron and  $0.6 M_{\odot}$  of Si-group elements, the corresponding kinetic energies of the ejecta would be  $E_{\text{kin}} = E_{\text{nuc}} - E_{\text{bind}} \simeq 0.83 \times 10^{51}$  and  $1.17 \times 10^{51}$  erg. Obviously, the nucleosynthesis yields depend on the actual  $Y_e$  and density profiles during explosive burning. If m1 achieves nuclear statistical equilibrium (NSE) before any significant expansion and deleptonization, then it would produce mostly stable iron-peak elements and  $\sim 0.3 M_{\odot}$  of  $^{56}\text{Ni}$ , resulting in a sub-luminous explosion that would resemble a SN Iax. Similarly low nickel masses would be expected if the deflagration wave never transitions to a detonation. On the other hand, if NSE is achieved at densities similar to our last MESA model, following an initial expansion (Figure 3), more than  $1 M_{\odot}$  of  $^{56}\text{Ni}$  can be produced, with only moderate amounts of iron. Similarly, m2 could produce up to  $1.3 M_{\odot}$  of iron elements if it does not expand any further.

## 3. Rates and delay times

An additional proxy for the potential connection between exploding (C)NeO cores and SNe Ia, is a comparison between their occurrence rates.

A zeroth-order upper bound on the number of stripped near-Chandrasekhar mass (C)NeO cores per unit solar mass of star formation,  $n_{\star}$ , is simply the number of stars,  $n_{\text{He}1.8-2.5}$ , that end up developing helium cores in the relevant mass range, here taken to be  $1.8 \lesssim M_{\text{He}}/M_{\odot} \lesssim 2.5$ , based on our simulations and the recent results of [Woosley \(2019\)](#) and [Farmer et al. \(2015\)](#) who also find that carbon ignites off-center in this mass range, independently of convective overshoot assumptions.

Based on [Farmer et al. \(2015\)](#), such helium stars originate from ZAMS stars with masses  $\sim 7 \dots 11 M_{\odot}$ . Adopting a [Chabrier \(2005\)](#) initial mass function (IMF), for the aforementioned mass range one finds,  $n_{\star} = n_{\text{He}1.8-2.5} \simeq 0.0059$ , which is larger than the observed number of SNe Ia per solar mass,  $n_{\text{SNIa}} \simeq 0.001-0.003$  (e.g. [Claeys et al. 2014a](#); [Maoz et al. 2014](#)). Here, one should keep in mind that the mass width for off-centre carbon burning is subject to several physical uncertainties, e.g. related to winds, as well as mixing and flame propagation during the carbon burning phase (Section 2). In addition, for isolated H-rich SAGB stars, the second dredge-up also limits the mass range for which the helium core mass remains near  $M_{\text{Ch}}$ , to about  $\sim 0.1 M_{\odot}$  around a ZAMS mass of  $11 M_{\odot}$  (c.f. Figure 1 in [Podsiadlowski et al. 2004](#)). Hence, more realistically, one would expect a maximum single-star contribution  $\sim 10$  times smaller than the rate estimated above. However, stars in interacting multiple systems, which lose their H-rich envelopes early, avoid dredge-up. Hence, most interacting stars capable of igniting carbon off-center will also manage to reach near- $M_{\text{Ch}}$  final core masses ([Podsiadlowski et al. 2004](#); [Poelarends 2007](#); [Poelarends et al. 2008](#); [Chen et al. 2014](#); [Meng & Podsiadlowski 2014](#); [Doherty et al. 2015](#); [Poelarends et al. 2017](#), and references therein).

If this channel is indeed mostly relevant to stars in multiple systems, *viz.* the hydrogen envelope can only be removed via binary interactions, then only the fraction of  $n_{\text{He}1.8-2.5}$  in interacting binaries is relevant. Adopting the same assumptions for the initial mass range as above,  $f_{\text{bin}} = 0.7$  for the fraction of stars in interacting binaries ([Sana et al. 2012](#)), a [Chabrier \(2005\)](#) IMF for the primaries (i.e. the initially more massive stars), and a mass-ratio distribution scaling as  $\propto q^{-0.1}$  ([Sana et al. 2012](#)), one finds  $n_{\star} \simeq 0.0038$ . Here, systems for which both stars have initial masses between 7 and  $11 M_{\odot}$  are only counted once, as the secondary would evolve in isolation once the primary explodes. Owing to the shape of the IMF, about 80% of the stars contributing to the former estimate are primaries, i.e. they would explode while still having a less-evolved companion.

More realistically, a significant number of these binaries would likely interact before the carbon-burning phase, thereby affecting the growth of the core and consequently the event rate. While detailed calculations are required to probe the influence of binary interactions, an upper limit on the expected rate can be obtained by comparing the frequency of progenitor systems relative to the SN Ib/c progenitors, assuming that the latter are dominated by stripped helium stars with masses  $\geq 2.5 M_{\odot}$  ([Woosley 2019](#)), which evolve similarly. Adopting the same IMF and initial mass range as above, one finds a total rate of  $\sim 0.8-1.0$  times the SN Ib/c rate, which is consistent with observations ([Branch & Wheeler 2017](#), and references therein).

Besides the total number of SNe Ia, a property that may be more challenging to match with observations is the evolution

of the SNIa rate with cosmic time. SNe Ia from such a channel would have delay times dominated by the main sequence lifetime of the progenitors, i.e. of order 30 to 78 Myr, for stars with ZAMS masses between 7 and 11  $M_{\odot}$ . Binaries interacting via early Case A RLO prior to the removal of the hydrogen envelope, could contribute events up to  $\sim 300$  Myr following star formation (corresponding to the MS lifetime of a 3.5  $M_{\odot}$  star). These delay times could help account for the high SNIa rates in star-forming galaxies, compared to ellipticals (Maoz & Badenes 2010; Claeys et al. 2014b), but some variant of the DD channel, or more generally a model in which the delay time much larger than the MS lifetime of intermediate-mass stars, would still be required to explain events with much longer delay times. However, if the (C)NeO core of a WD were to evolve in a similar way due to mass accretion from a companion as in the SD scenarios, or in a merger similar to the DD and CD scenarios, then the corresponding explosion could contribute a SNIa several Gyrs after star formation (see also Kashi & Soker 2011; Chen et al. 2014; Meng & Podsiadlowski 2014; Marquardt et al. 2015; Schwab et al. 2015; Jones et al. 2016; Schwab et al. 2017; Schwab & Rocha 2019; Kashyap et al. 2018; Augustine et al. 2019; Soker 2019, and references therein). Finally, if (C)NeO explosions produce less nickel than typical SNe Ia, then the short delay times would match those of under-luminous SNeIax which predominantly occur in star-forming regions (Lyman et al. 2013; Jha 2017).

#### 4. Summary

We have shown that at least some stars capable of developing near- $M_{\text{Ch}}$  (C)NeO cores after losing their hydrogen envelopes, may explode as SNe Ia instead of undergoing a core-collapse ECSN. For NeO compositions, the runaway seems to be triggered by the ignition of residual carbon following electron captures on  $^{24}\text{Mg}$ , which in turn leads to explosive oxygen burning at densities below  $5.9 \times 10^9 \text{ g cm}^{-3}$  (Sections 2). For hybrid CO/NeO cores, ignition is triggered by core compression, at a density of  $1.8 \times 10^9 \text{ g cm}^{-3}$ , similar to what is expected for CO WD deflagrations. For either case, the conditions at the onset of oxygen burning are such that the energetics could resemble closely a typical SNIa, or an under-luminous Iax depending on when and if the initial deflagration transitions into a detonation (Section 2.5). It would be worth considering whether the differences in initial density and composition could lead to distinct nucleosynthetic signatures that would help distinguish these progenitors and/or contribute uniquely to the chemical evolution of the Galaxy (in analogy to Jones et al. 2019, for ECSNe).

The frequency of the corresponding progenitor systems is sufficient to account for a considerable fraction of the observed SNIa rate. Our optimistic zeroth-order upper bounds in Section 3 suggest that SNe Ia from non-accreting progenitors could occur at the same rate as SNe Ib/c, assuming that the latter also result from stripped helium stars. Since, the bulk of events would occur only  $\sim 50$  Myr after star formation, this channel is mostly relevant to star-forming galaxies. The shorter delay times compared to traditional SNIa scenarios, open further interesting avenues for constraining this model, e.g. by considering the abundance ratios of alpha elements relative to iron in metal-poor stars.

While here we demonstrate that the helium envelope is likely lost only after the core has grown to  $M_{\text{Ch}}$ , its evolution remains a major uncertainty for this progenitor channel. If helium is removed sufficiently early, e.g. due to binary interactions, then sub- $M_{\text{Ch}}$  (C)NeO WDs would be formed instead.

In spite of the mass-loss uncertainties, if viable, this channel would help explain some of the observed SNIa diversity. Since either star in a binary system may potentially explode as a SNIa without accreting from its companion, the resulting events can resemble setups expected in all SD and DD/CD scenarios. Explosions of secondaries, would follow a first core-collapse SN. This could lead to SNIa remnants with no luminous surviving stars, high proper motions due to a kick from the first SN (like the Kepler SN remnant, Chiotellis et al. 2012), and possibly associated with a neutron star. Since the envelope can be removed either due to winds, case-BB mass transfer, or a common envelope event, some diversity is also expected in the SN environment. In turn this would influence both the appearance of the explosion and the evolution of the SN remnant. The rates estimated in Section 3 are also broadly consistent with the number of SNe Ia that seem to explode inside planetary nebulae ( $\sim 20\%$ ; Tsebrenko & Soker 2015).

*Acknowledgements.* We thank the referee for the extremely helpful report. This research made extensive use of NASA's ADS, MESA<sup>2</sup> (Paxton et al. 2011, 2013, 2015, 2018) and Astropy<sup>3</sup> (Astropy Collaboration & Astropy Contributors 2018). Figure 1 was created with NuGridPy<sup>4</sup>

#### References

- Arnett, W. D. 1969, *The Astrophysical Journal Supplement Series*, 5, 180
- Astropy Collaboration, & Astropy Contributors. 2018, *The Astronomical Journal*, 156, 123
- Augustine, C. N., Willcox, D. E., Brooks, J., Townsley, D. M., & Calder, A. C. 2019, arXiv e-prints, 1910, arXiv:1910.12403
- Bochenek, C. D., Dwarkadas, V. V., Silverman, J. M., et al. 2018, *Monthly Notices of the Royal Astronomical Society*, 473, 336
- Branch, D., Baron, E., Thomas, R. C., et al. 2004, *Publications of the Astronomical Society of the Pacific*, 116, 903
- Branch, D., & Wheeler, J. C. 2017, *Supernova Explosions: Astronomy and Astrophysics Library*, ISBN 978-3-662-55052-6. Springer-Verlag GmbH Germany, 2017
- Chabrier, G. 2005, *The Initial Mass Function 50 Years Later*, 327, 41
- Chanlaridis, S., Antoniadis, J., Gräfener, G., & Langer, N. 2019, in prep.
- Chen, M. C., Herwig, F., Denissenkov, P. A., & Paxton, B. 2014, *Monthly Notices of the Royal Astronomical Society*, 440, 1274
- Chiotellis, A., Schure, K. M., & Vink, J. 2012, *Astronomy & Astrophysics*, 537, A139
- Churazov, E., Sunyaev, R., Isern, J., et al. 2014, *Nature*, 512, 406
- Claeys, J. S. W., Pols, O. R., Izzard, R. G., Vink, J., & Verbunt, F. W. M. 2014a, *Astronomy & Astrophysics*, 563, A83
- . 2014b, *Astronomy and Astrophysics*, 563, A83
- Cox, J. P., & Giuli, R. T. 1968, *Principles of stellar structure*
- Cyburtt, R. H., Amthor, A. M., Ferguson, R., et al. 2010, *The Astrophysical Journal Supplement Series*, 189, 240
- Denissenkov, P. A., Herwig, F., Truran, J. W., & Paxton, B. 2013, *The Astrophysical Journal*, 772, 37
- Doherty, C. L., Gil-Pons, P., Siess, L., Lattanzio, J. C., & Lau, H. H. B. 2015, *Monthly Notices of the Royal Astronomical Society*, 446, 2599
- Farmer, R., Fields, C. E., & Timmes, F. X. 2015, *The Astrophysical Journal*, 807, 184
- Filippenko, A. V., Richmond, M. W., Matheson, T., et al. 1992, *The Astrophysical Journal*, L5
- Gräfener, G., Owocki, S. P., Grassitelli, L., & Langer, N. 2017, *A&A*, 608, A34
- Grevesse, N., & Sauval, A. J. 1998, *Space Science Reviews*, 85, 161
- Gutierrez, J., Garcia-Berro, E., Iben, I., et al. 1996, *The Astrophysical Journal*, 459, 701
- Harris, C. E., Nugent, P. E., & Kasen, D. N. 2016, *The Astrophysical Journal*, 823, 100
- Howell, D. A., Sullivan, M., Nugent, P. E., et al. 2006, *Nature*, 443, 308
- Iben, Jr., I., & Renzini, A. 1983, *Annual Review of Astronomy and Astrophysics*, 21, 271
- Jha, S. W. 2017, *Handbook of Supernovae*, 375

<sup>2</sup> <http://mesastar.org>

<sup>3</sup> <http://www.astropy.org>

<sup>4</sup> <https://github.com/NuGrid/NuGridPy>

- Jones, S., Röpke, F. K., Pakmor, R., et al. 2016, *Astronomy & Astrophysics*, 593, A72
- Jones, S., Röpke, F. K., Fryer, C., et al. 2019, *Astronomy and Astrophysics*, 622, A74
- Kasen, D. 2010, *The Astrophysical Journal*, 708, 1025
- Kashi, A., & Soker, N. 2011, *Monthly Notices of the Royal Astronomical Society*, 417, 1466
- Kashyap, R., Haque, T., Lorén-Aguilar, P., García-Berro, E., & Fisher, R. 2018, *The Astrophysical Journal*, 869, 140
- Kippenhahn, R., Ruschenplatt, G., & Thomas, H.-C. 1980, *Astronomy and Astrophysics*, 91, 175
- Langer, N., Fricke, K. J., & Sugimoto, D. 1983, *Astronomy and Astrophysics*, 126, 207
- Lecoanet, D., Schwab, J., Quataert, E., et al. 2016, *The Astrophysical Journal*, 832, 71
- Li, W., Filippenko, A. V., Chornock, R., et al. 2003, *Publications of the Astronomical Society of the Pacific*, 115, 453
- Livio, M., & Mazzali, P. 2018, *Physics Reports*, 736, 1
- Lyman, J. D., James, P. A., Perets, H. B., et al. 2013, *Monthly Notices of the Royal Astronomical Society*, 434, 527
- Magee, M. R., Sim, S. A., Kotak, R., Maguire, K., & Boyle, A. 2019, *Astronomy and Astrophysics*, 622, A102
- Magee, M. R., Kotak, R., Sim, S. A., et al. 2016, *Astronomy and Astrophysics*, 589, A89
- Maoz, D., & Badenes, C. 2010, *Monthly Notices of the Royal Astronomical Society*, 407, 1314
- Maoz, D., Mannucci, F., & Nelemans, G. 2014, *Annual Review of Astronomy and Astrophysics*, 52, 107
- Marquardt, K. S., Sim, S. A., Ruiter, A. J., et al. 2015, *Astronomy and Astrophysics*, 580, A118
- Meng, X., & Podsiadlowski, P. 2014, *apj*, 789, L45
- Nomoto, K. 1982, *The Astrophysical Journal*, 253, 798
- Nomoto, K., & Kondo, Y. 1991, *The Astrophysical Journal*, 367, L19
- Owocki, S. P., Gayley, K. G., & Shaviv, N. J. 2004, *The Astrophysical Journal*, 616, 525
- Paxton, B., Bildsten, L., Dotter, A., et al. 2011, *The Astrophysical Journal Supplement Series*, 192, 3
- Paxton, B., Cantiello, M., Arras, P., et al. 2013, *The Astrophysical Journal Supplement Series*, 208, 4
- Paxton, B., Marchant, P., Schwab, J., et al. 2015, *The Astrophysical Journal Supplement Series*, 220, 15
- Paxton, B., Schwab, J., Bauer, E. B., et al. 2018, *The Astrophysical Journal Supplement Series*, 234, 34
- Podsiadlowski, P., Langer, N., Poelarends, A. J. T., et al. 2004, *The Astrophysical Journal*, 612, 1044
- Poelarends, A. J. T. 2007, PhD thesis
- Poelarends, A. J. T., Herwig, F., Langer, N., & Heger, A. 2008, *The Astrophysical Journal*, 675, 614
- Poelarends, A. J. T., Wurtz, S., Tarka, J., Cole Adams, L., & Hills, S. T. 2017, *The Astrophysical Journal*, 850, 197
- Rose, W. K. 1969, *The Astrophysical Journal*, 155, 491
- Ruiz-Lapuente, P., Jeffery, D. J., Challis, P. M., et al. 1993, *Nature*, 365, 728
- Sana, H., de Mink, S. E., de Koter, A., et al. 2012, *Science*, 337, 444
- Sato, Y., Nakasato, N., Tanikawa, A., et al. 2015, *The Astrophysical Journal*, 807, 105
- Schwab, J., Bildsten, L., & Quataert, E. 2017, *Monthly Notices of the Royal Astronomical Society*, 472, 3390
- Schwab, J., Quataert, E., & Bildsten, L. 2015, *Monthly Notices of the Royal Astronomical Society*, 453, 1910
- Schwab, J., & Rocha, K. A. 2019, *The Astrophysical Journal*, 872, 131
- Seitenzahl, I. R., & Townsley, D. M. 2017, *Nucleosynthesis in Thermonuclear Supernovae*, 1955
- Siess, L. 2006, *Astronomy and Astrophysics*, 448, 717
- Smith, N., & Owocki, S. P. 2006, *ApJ*, 645, L45
- Soker, N. 2019, arXiv e-prints, 1912, arXiv:1912.01550
- Suzuki, T., Toki, H., & Nomoto, K. 2016, *The Astrophysical Journal*, 817, 163
- Takahashi, K., Yoshida, T., & Umeda, H. 2013, *The Astrophysical Journal*, 771, 28
- Taubenberger, S. 2017, *Handbook of Supernovae*, 317
- Tsebrenko, D., & Soker, N. 2015, *Monthly Notices of the Royal Astronomical Society*, 447, 2568
- van Kerkwijk, M. H., Chang, P., & Justham, S. 2010, *The Astrophysical Journal*, 722, L157
- Vink, J. S. 2017, *Astronomy and Astrophysics*, 607, L8
- Waldman, R., & Barkat, Z. 2006, Ph.D. Thesis
- Waldman, R., Yungelson, L. R., & Barkat, Z. 2008, in *Astronomical Society of the Pacific Conference Series*, Vol. 391, *Hydrogen-Deficient Stars*, ed. A. Werner & T. Rauch, 359
- Wang, B., & Han, Z. 2012, *New Astronomy Reviews*, 56, 122
- Wheeler, J. C. 1978, *The Astrophysical Journal*, 225, 212
- Woosley, S. E. 2019, *The Astrophysical Journal*, 878, 49
- Yoon, S.-C. 2017, *Monthly Notices of the Royal Astronomical Society*, 470, 3970